

Texture Evolution of a Non-oriented Electrical Steel Cold Rolled at Directions Different from the Hot Rolling Direction



YOU LIANG HE, ERIK HILINSKI, and JIAN LI

With the objective of optimizing the crystallographic texture of non-oriented electrical steel, *i.e.*, reducing the $\langle 111 \rangle // \text{ND}$ and $\langle 110 \rangle // \text{RD}$ fibers and promoting the $\langle 001 \rangle // \text{ND}$ texture, a new rolling scheme was proposed and tested, in which the cold rolling direction (CRD) was intentionally inclined at an angle to the hot rolling direction (HRD) in order to change the orientation flow paths during cold rolling and alter the final texture of the annealed sheets. A non-oriented electrical steel containing 0.88 wt pct Si was hot rolled using conventional routes and annealed, and a number of rectangular plates were cut from the hot band with the longitudinal directions inclined at various angles, *i.e.*, 0, 15, 30, 45, 60, 75, and 90 deg, to the HRD. These plates were then cold rolled along the longitudinal directions with a thickness reduction of 72 pct. The cold-rolled samples were annealed, temper rolled and annealed again (final annealing). The texture evolution during hot rolling, hot band annealing, cold rolling, and final annealing was characterized by electron backscatter diffraction and X-ray diffraction techniques. By changing the CRD with respect to the HRD, the initial texture and the orientation flow paths were altered, which resulted in apparent differences in the textures as compared to conventional cold rolling. After temper rolling and final annealing, the recrystallization textures consisted of mainly a $\langle 001 \rangle // \text{ND}$ fiber and there was almost no $\langle 111 \rangle // \text{ND}$ fiber. The sample cold rolled at an angle of 60 deg to the HRD had the strongest texture (intensity almost $2 \times$ of conventional rolling) with a maximum at the cube $\{001\} \langle 100 \rangle$ orientation—a magnetically favorable orientation for non-oriented electrical steels.

DOI: 10.1007/s11661-015-3136-5

© The Minerals, Metals & Materials Society and ASM International 2015

I. INTRODUCTION

NON-ORIENTED electrical steels are widely used in electric motors, generators, alternators, *etc.* as the core material to amplify the magnetic field generated by electric current (in motors)^[1] or to enhance electric current generation (in generators). The energy efficiency of electric motors or generators is closely related to the magnetic properties of the core lamination, which in turn is dependent on the crystallographic texture of the processed electrical steel sheets. The ideal crystallographic texture for optimum magnetic properties is the $\langle 001 \rangle // \text{ND}$ fiber (or the θ -fiber, which includes the ideal orientations of cube, $\{001\} \langle 100 \rangle$, and rotated cube, $\{001\} \langle 110 \rangle$), because these orientations

have two easy magnetisation $\langle 001 \rangle$ directions uniformly spreading in the sheet plane.^[2] However, this fiber texture is usually difficult to obtain through conventional hot rolling, cold rolling, and annealing processes.^[3]

During the manufacturing of non-oriented electrical steel sheets through casting, hot rolling, cold rolling, and annealing, the initial preferred crystal orientations created by solidification from the melt will be altered a few times by the thermomechanical processing (TMP) procedures that follow, which involve several texture development mechanisms such as plastic deformation, phase transformation, and recrystallization.^[4] The texture in hot rolled and annealed strip is mainly determined by rolling temperature, coiling conditions, and hot band annealing parameters.^[5–8] The chemical composition also plays an important role through its influence on phase transformation: grades with higher than 2.5 pct Si concentration usually do not have an austenite phase, while alloys with less than 2.5 pct Si normally have an austenite to ferrite transformation.^[9,10] The cold rolling texture is mainly dependent on the initial texture, reduction rate and whether intermediate annealing is applied between cold rolling steps or not.^[11,12] The final annealing texture is, to a large extent, determined by the cold rolling texture as well as the annealing conditions such as temperature, atmosphere, heating and cooling rates, holding time,

YOU LIANG HE and JIAN LI, Research Scientists, are with CanmetMATERIALS, Natural Resources Canada, 183 Longwood Road South, Hamilton, ON L8P 0A5, Canada. Contact e-mail: youliang.he@canada.ca ERIK HILINSKI, Director-Steel Technology, formerly with the Research and Technology Center, United States Steel Corporation, Munhall, PA, is now with Tempel Steel Co., Chicago, IL.

The following copyright notice pertains only to Youliang He and Jian Li: Printed by permission of Her Majesty the Queen in Right of Canada, as represented by the Director General of the Policy and Planning Branch, Innovation and Energy Technology Sector, Natural Resources Canada.

Manuscript submitted November 14, 2014.

Article published online September 8, 2015

continuous or batch annealing,^[13–18] *etc.* Although a wide range of these processing parameters were varied in many investigations, limited variations in the final texture and magnetic quality had been produced.^[19] The ideal cube texture {001}<100> has rarely been realized in the final non-oriented electrical steel sheets through conventional rolling and annealing processes.

One method that was reported to have produced a strong cube texture was by cross-rolling,^[19,20] *i.e.* the hot-rolled sheet was rotated 90 deg before cold rolling, which means that the cold rolling direction (CRD) was perpendicular to the hot rolling direction (HRD). However, cross rolling of sheet steel is virtually impossible to implement in a continuous manufacturing line and thus has no industrial application. In the present study, a new cold rolling scheme is proposed, *i.e.*, the CRD is inclined at an angle between 0 and 90 deg to the HRD. This rolling scheme differs from cross rolling in that the steel sheet may be continuously (or at least semi-continuously) processed, while in cross rolling, only very short sheets can be produced in a batch mode because of the limitation of the roll width. Due to the inclined angle between CRD and HRD, the initial texture and the orientation flow paths during cold rolling are different from either conventional rolling or cross rolling, which is expected to generate different cold rolling and final annealing textures.

II. MATERIAL AND EXPERIMENTAL PROCEDURES

The chemical composition of the investigated non-oriented electrical steel is given in Table I. The steel was melted in a laboratory vacuum induction furnace and cast into 200 mm × 200 mm ingots. After removal from the ingot mold, the material was reheated to a nominal temperature of 1311 K (1038 °C) and hot rolled from 200 to 25 mm (thickness) in 6 passes on a 2-high reversing laboratory rolling mill. The two surfaces of the plates were machined in a lathe to remove 3.1 mm of material (oxides) from each side. The plates were reheated again to 1311 K (1038 °C) and further hot rolled down to a thickness of ~2.3 mm in 4 passes with a total reduction rate of ~90 pct. Following the second hot rolling step, the tertiary scale on the surfaces was removed by batch pickling in heated HCl acid at about 355 K (82 °C). The plates were then annealed at 1113 K (840 °C) for 60 hours in a dry 100 pct hydrogen atmosphere.

The annealed steel plates were cut to smaller rectangular pieces (50 mm × 180 mm) at various angles to the HRD (Figure 1). In this way, the CRDs were inclined 0, 15, 30, 45, 60, 75, and 90 deg to the original HRD. These smaller pieces were cold rolled to 0.65-mm-thick strips in multiple passes using a reversing laboratory rolling

mill. The cold-rolled strips were then annealed at 1073 K (800 °C) for 30 seconds in an Ar atmosphere. The samples were cold rolled again (temper rolling) with approximately 2 pct reduction to straighten and flatten the material, and finally annealed at 1053 K (780 °C) for 2 hours in an argon protected environment.

The microstructure of the cold-rolled and annealed sheets were characterized by optical microscopy. The samples were prepared using conventional metallographic techniques and etched with a 2 pct Nital solution. Grain size measurements were conducted in accordance with ASTM E112-12 by using the Heyn Lineal Intercept procedure.^[21] EBSD samples were prepared by regular grinding using 320, 400, and 600 grit SiC papers and polishing with 9, 3, and 1 μm diamond pastes, followed by a final polishing step with a 0.05 μm colloidal silica solution. The EBSD scans were performed in a field emission gun scanning electron microscope (FEG-SEM) (Nova NanoSEM, FEI) equipped with an OIM 6.1 EBSD system (EDAX).

Macrotexture measurements were conducted using a Bruker D8 DISCOVER X-ray Diffraction Goniometer (with a Vantec 500 area detector) operated at 35 kV and 45 mA (Co-Kα X-ray, λ = 1.79026 Å). The samples were prepared by grinding the sheet plane from the top surface down to approximately 1/2 of the thickness (middle plane). After polishing using 9 and 3 μm diamond solutions, the surfaces were etched for 1 minute in a solution of 100 ml distilled water and 7 ml HF. During measurements, the samples were oscillated in the X and Y, or RD and TD directions by ±7 and ±5 mm, respectively. Thus, an area of approximately 14 × 10 mm² per sample was scanned to capture the diffraction data. Three incomplete pole figures, (200), (110), and (211), were measured and the Orientation Density Functions (ODF) were calculated from these pole figures using the MTEX (V3.4.2) software.^[22] This code was used because it is suited for analyzing high-resolution diffraction pole figures measured by area detectors. In the ODF calculations, pole figure data with a tilt angle greater than 75 deg were omitted. All the calculations were carried out using the de la Vallée Poussin kernel with a halfwidth of 5 deg and a resolution of 5 deg. The volume fractions of the ideal texture components or fibers were calculated from the ODF within 15 deg from the exact orientations in Euler space.

III. RESULTS

A. Hot Rolling and Annealing

The alloying elements (*e.g.* Si, Al, Mn, and P) in electrical steels have a considerable effect on the phase transformation behavior,^[23] which in turn impacts the

Table I. Chemical Composition of the Investigated Steel (wt pct)

C	Mn	P	S	Si	Al	Fe
0.002	0.31	0.01	0.001	0.88	0.46	balance

hot-rolling microstructure and texture of the steel. In practice, the Fe-(Si + 2Al) phase diagram is commonly used to replace the equilibrium Fe-Si phase diagram to investigate the hot-rolling process of electrical steels.^[9] Figure 2 shows the Fe-rich portion of the Fe-(Si + 2Al) phase diagram with superimposed dynamic A_{r3} and A_{r1} critical temperatures.^[9] The steel used in this study contains 0.88 wt pct of Si and 0.46 wt pct of Al, thus the Si + 2Al content is 1.80 wt pct. It is apparent that, if only the alloy element Si is considered, the material will go through a complete austenite region as well as an austenite (γ) + ferrite (α) two-phase zone when cooling down to the full ferrite area. With the effect of Al, the material no longer has a complete austenite zone and will only go through the $\gamma + \alpha$ region during cooling to ferrite.

In this study, the steel plates were reheated to 1311 K (1038 °C) and the hot rolling was conducted at temperatures between ~1203 K and ~893 K (~930 °C and ~620 °C) in a total of four passes. The entry and exit temperatures for the four passes were approximately (1203 K, 1163 K), (1153 K, 1113 K), (1073 K, 1008 K),

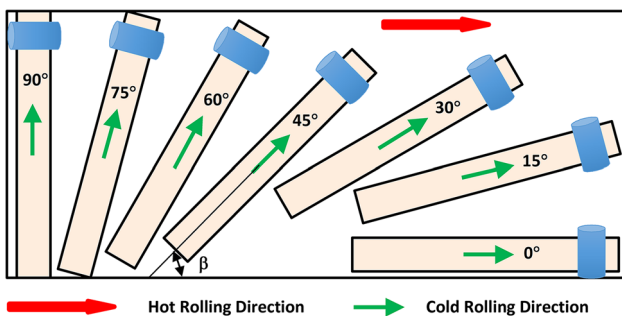


Fig. 1—Schematic illustration of the cutting of cold-rolling samples from a hot-rolled plate.

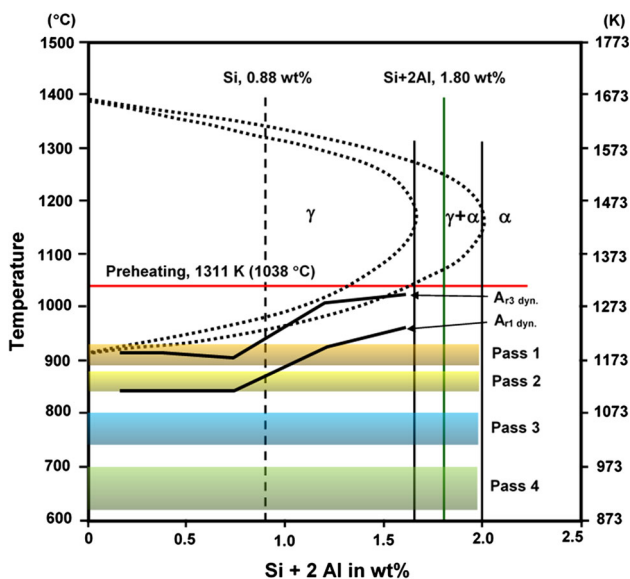


Fig. 2—Fe-rich portion of the Fe-(Si + 2Al) phase diagram superimposed by the dynamic A_{r3} and A_{r1} critical temperatures.^[9] The start and finish temperatures for the 4 hot rolling passes are also shown.

(973 K, 893 K) [(930 °C, 890 °C), (880 °C, 840 °C), (800 °C, 735 °C), and (700 °C, 620 °C)], respectively, as shown in Figure 2. It is seen that due to the effect of Al, the hot rolling was actually performed below the phase transformation temperature (*i.e.*, below the dynamic A_{r3} and A_{r1}). Thus, the austenite in the reheated microstructure has transformed to ferrite before rolling deformation, and the textures obtained are those of hot-rolled ferrite.

Figure 3(a) illustrates the cross-sectional microstructure and microtexture after hot rolling. The microstructure mainly consists of large, elongated grains and shows apparent orientation variations within the grains as depicted by the slightly different colors within these crystals. This was resulted from the plastic deformation on those grains during hot rolling, which caused the reorientation of the crystals. The variation of orientations within these crystals is usually low, *i.e.*, less than 2 to 5 deg. There are much smaller but again elongated grains in the microstructure, indicating the occurrence of dynamic recrystallization and the deformation of the recrystallized microstructure. The colors of the inverse pole figure map show that a majority of the grains have their {001} and {011} planes (red and green, respectively) perpendicular to the normal direction (ND). The calculated orientation distribution functions show that these mainly correspond to the cube, rotated cube and Goss texture components (Figures 3(b) and (c)). Although these components are favorable crystallographic textures for good magnetic properties, as will be seen, they tend to be altered after hot band annealing, cold rolling, temper rolling, and final annealing.

Figure 4 shows the microstructure and microtexture of the hot-rolled electrical steel after annealing at 1113 K (840 °C) for 60 hours. Although with a very long holding time at a relatively high temperature, the recrystallized microstructure is still inhomogeneous: grain sizes vary from ~20 to ~550 μm (Figure 4(d)), which indicates inhomogeneous grain growth of different grains. The calculated ODF's (Figures 4(b) and (c)) show that the {001}\{100\}, {001}\{110\}, and {011}\{100\} textures observed in the hot-rolled sample essentially diminished, while a {001}\{140\} orientation, which is located between the cube and rotated cube in the $\langle 001 \rangle // \text{ND}$ fiber (θ -fiber), appeared. The strongest component is an uncommon orientation, $\left\{0\frac{1}{2}\frac{\sqrt{3}}{2}\right\}\left\{\frac{1}{2}\frac{3}{4}\frac{\sqrt{3}}{4}\right\}$, on the $\varphi_2 = 0$ deg section. Another relatively strong orientation is {110}\{665\}, which is located between the {110}\{110\} (rotated Goss) and the {110}\{112\} (brass) along the $\langle 110 \rangle // \text{ND}$ fiber. A few peaks (*e.g.*, {111}\{451\}, {111}\{132\}, and {667}\{3 11 12\}) near the γ -fiber are also found, which were not seen in the hot-rolled plate. Compared to hot rolling, the overall texture is weakened after annealing.

B. Cold-Rolling Microstructure and Texture

Figure 5 shows the microstructures of the samples cold rolled at various angles (0 to 90 deg) with respect to the HRD. The variation in etching color indicates

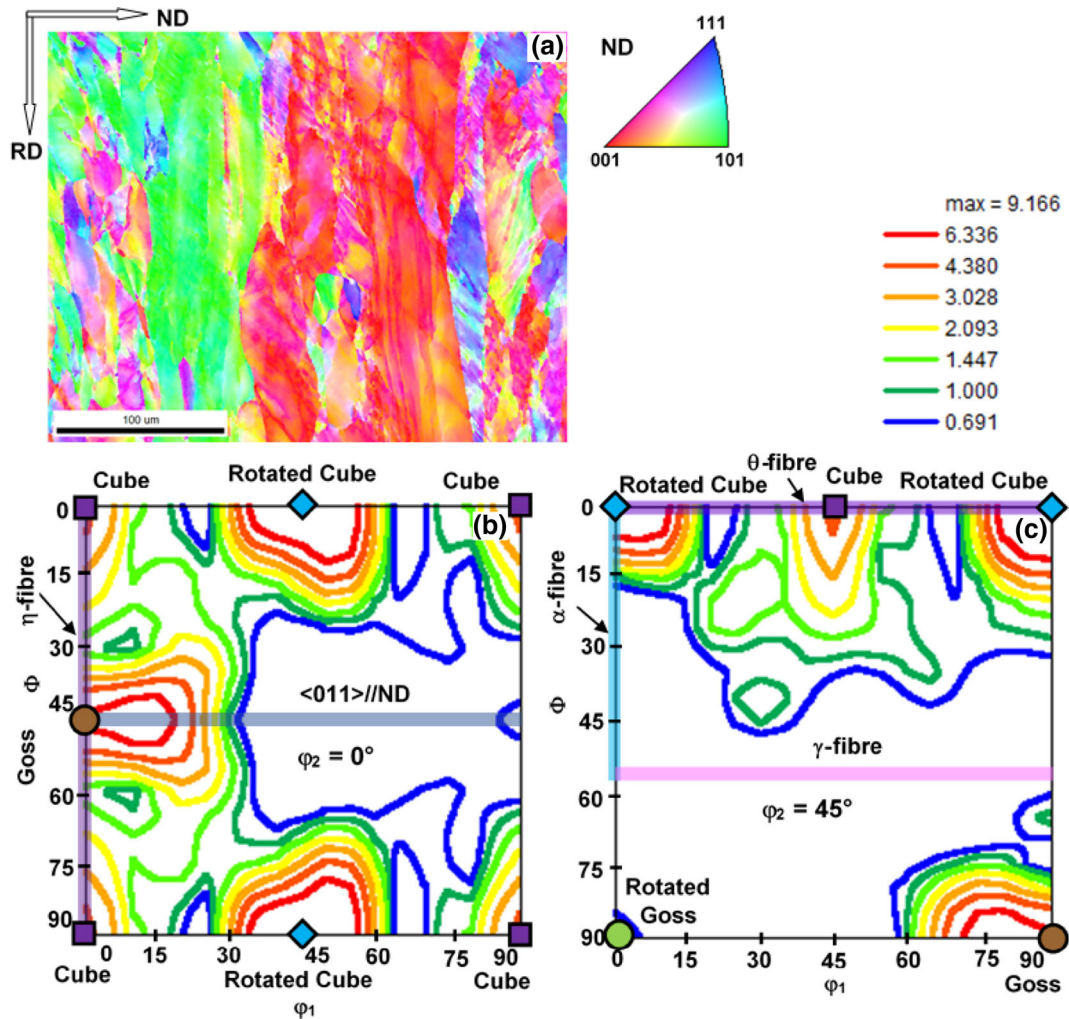


Fig. 3—Microtexture and microstructure after hot rolling: (a) inverse pole figure map, (b) $\phi_2 = 0$ deg section of the calculated ODF from the EBSD scan (Bunge notation), (c) $\phi_2 = 45$ deg section of the ODF. Some relevant texture components and fibers are marked on the respective sections. Cube: $\{001\}\langle 100 \rangle$, Rotated Cube: $\{001\}\langle 110 \rangle$, Goss: $\{110\}\langle 001 \rangle$, Rotated Goss: $\{110\}\langle 110 \rangle$, η -fiber: $\langle 001 \rangle // \text{RD}$, θ -fiber: $\langle 100 \rangle // \text{ND}$, α -fiber: $\langle 110 \rangle // \text{RD}$, γ -fiber: $\langle 111 \rangle // \text{ND}$.

inhomogeneous plastic deformation on different regions: grains lightly etched have less dislocation density and experienced relatively uniform plastic deformation, while darkly etched regions imply massive collection of dislocations (shear bands) induced by highly concentrated, inhomogeneous plastic flow. Although the variation of the CRD with respect to the HRD does not result in significant difference in the cold-rolled microstructure, samples cold rolled at 45 and 75 deg angles to the HRD seem to have the most shear bands (dark regions), while those rolled at 15 and 60 deg angles have the least deformation bands.

The inclination of the CRD at an angle to the HRD is equivalent to rotating the sample around the normal direction (ND) by a certain angle (β) with respect to the rolling direction (RD), which results in the alteration of the initial texture of the sample. Using the MTEX software,^[22] the annealed hot band orientations measured by EBSD (Figure 4(a)) were rotated by 15, 30, 45, 60, 75, and 90 deg, and the computed orientation density functions are shown in Figure 6. It is noted that some

rotations not only altered the character of the texture, but they also considerably changed the intensity of the texture. For example, after rotating by 30, 60, and 75 deg, the intensities of the texture were considerably increased. The apparent difference in the intensities was caused by the application of a pseudo-orthorhombic sample symmetry during the calculations of the ODF, which actually was not true for rotations other than 90 deg. The intensities of 0 and 90 deg inclination are the same since the rotation of 90 deg around the normal direction is an element of the orthorhombic sample symmetry.

The textures (measured by XRD) after cold rolling at 0, 15, 30, 45, 60, 75, and 90 deg to the HRD are shown in Figure 7. Although the initial textures differ considerably, the cold-rolled textures all consist of a similar overall range of preferred orientations typical of bcc metals after rolling, *i.e.*, the γ - and α -fibers, or the $\langle 111 \rangle // \text{ND}$ and $\langle 110 \rangle // \text{RD}$ fibers.^[4,24] However, the initial texture has a strong effect on the intensity and orientation distribution within that range. A strong

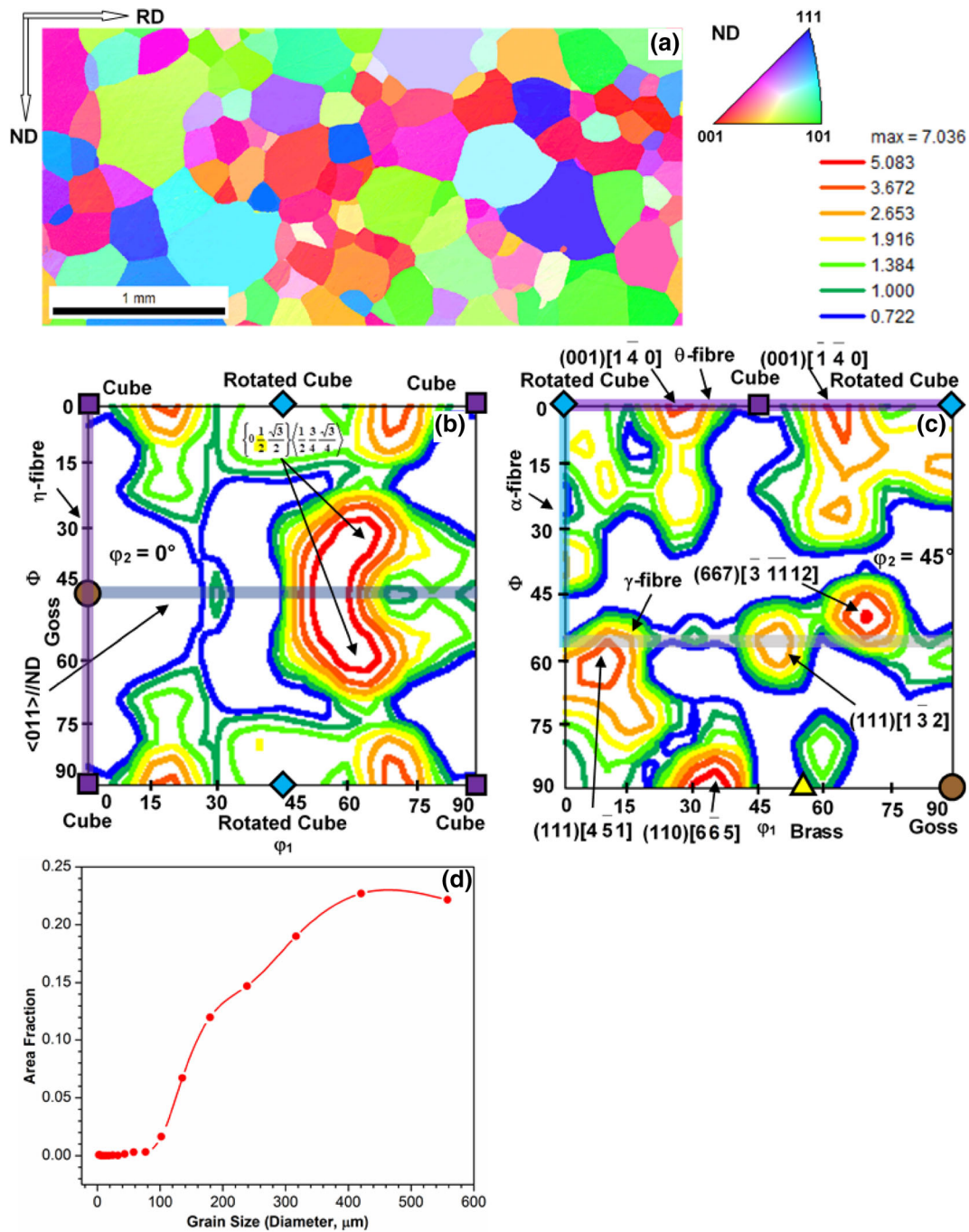


Fig. 4—Microtexture and microstructure after hot rolling and annealing: (a) inverse pole figure map, (b) $\phi_2 = 0$ deg section of the calculated ODF from the EBSD scan, (c) $\phi_2 = 45$ deg section of the ODF, and (d) grain size distribution.

$\{001\}\langle 110 \rangle$ (rotated cube) texture is observed in all the samples, although the relative intensities with respect to the $\{112\}\langle 110 \rangle$ component are different.

At a 0 deg angle (*i.e.*, conventional rolling), the texture consists of strong $\{001\}\langle 110 \rangle$ and $\{112\}\langle 110 \rangle$ orientations, together with the $\langle 110 \rangle // \text{RD}$ and $\langle 111 \rangle // \text{ND}$ fibers. These features are very similar to those usually observed in cold-rolled low carbon steels and electrical steels.^[4,24] The $\{001\}\langle 110 \rangle$ component has the maximum intensity in all the inclination angles except at

30 deg, where an intensity maximum develops at the $\{112\}\langle 110 \rangle$ orientation. The $\{112\}\langle 110 \rangle$ component is the stable final orientation for plane-strain compression (rolling) as predicted by the full constraint Taylor model.^[4,25,26] This theoretically stable orientation (in conventional rolling) is not preserved when the inclination angle increases to 75 and 90 deg, where the dominant texture is rotated cube and no obvious peak is observed at the $\{112\}\langle 110 \rangle$ position. It should also be noted that inclining the CRD to HRD tends to change

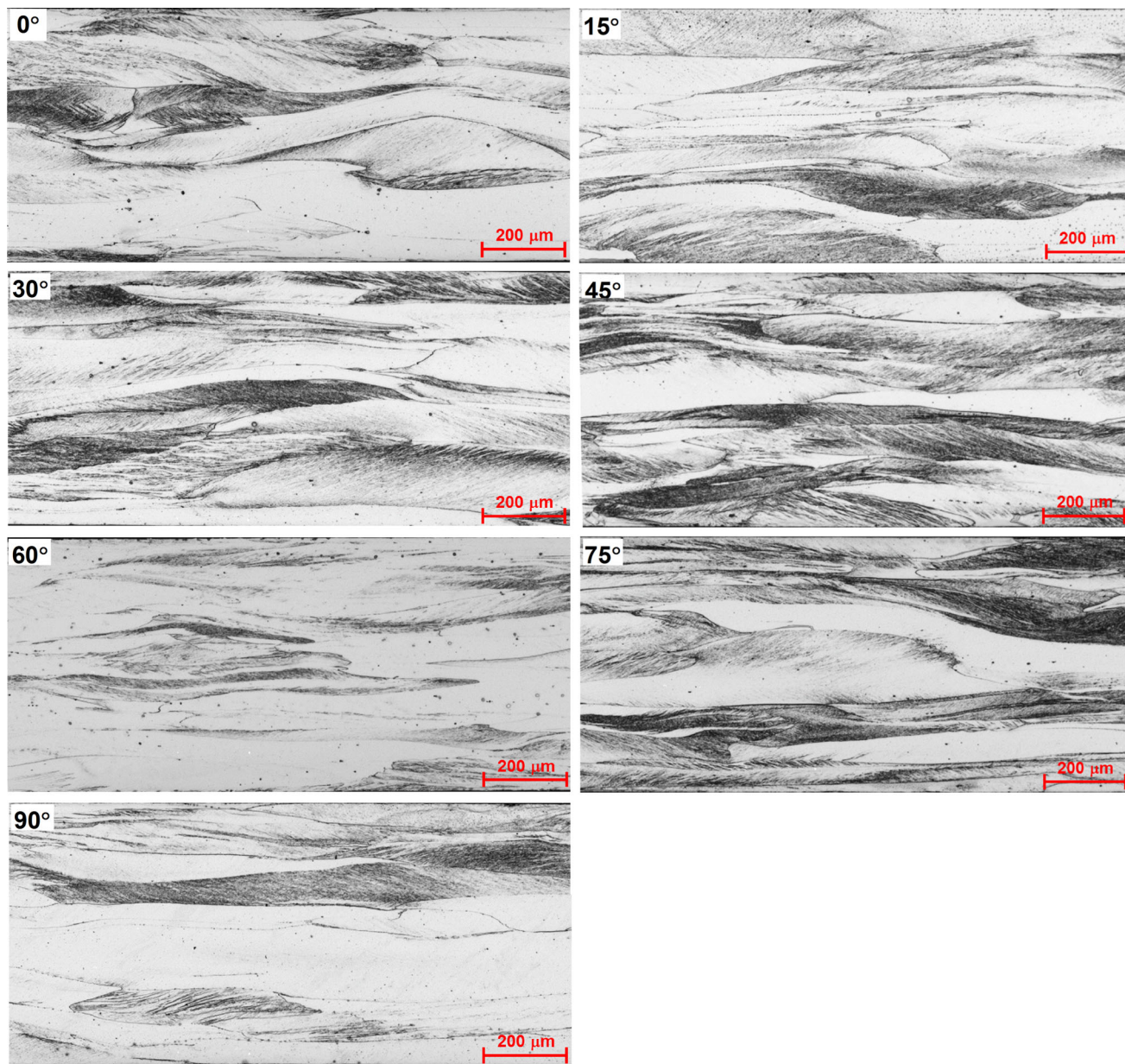


Fig. 5—Optical micrographs (cross section) of samples cold rolled at various angles with respect to the hot rolling direction.

the continuous γ fiber normally observed in conventional rolling (0 deg) into discrete peaks at $\{111\}\langle 011\rangle$.

The inclination of the CRD to HRD also sharpens the cold-rolling texture: when the angle is 0 deg (conventional rolling) the maximum texture intensity is about 7, while at an angle of 75 deg, the maximum intensity increases to 16 (*i.e.*, more than doubled). Cross rolling (with an angle of 90 deg) produces the second strongest cold-rolling texture, with a maximum intensity of 12. At all the other angles, the textures are strengthened, but to a lesser extent.

The variation of intensity along the α - and γ -fibers with respect to the inclination angle is shown in Figure 8. It is seen from Figure 8(a) that inclining the CRD to the HRD intensifies the rotated cube component in all angles. At angles of 30 and 60 deg, the $\{112\}\langle 110\rangle$ component is also

considerably strengthened, while at 75 and 90 deg the intensity of $\{112\}\langle 110\rangle$ is significantly decreased. The 75 deg inclination produces the strongest $\{001\}\langle 110\rangle$ texture, and the 90 deg angle leads to the lowest $\{112\}\langle 110\rangle$ intensity. An inclination angle of 45 deg has some moderate effect on the α fiber, while the 15 deg angle only imposes a minor effect on the texture development.

The distribution of intensity along the γ -fiber (Figure 8(b)) resembles a cosine wave curve (due to the symmetry of the twin-related orientations) from $\varphi_1 = 0$ deg to $\varphi_1 = 90$ deg, with maxima at $\{111\}\langle 110\rangle$ and minima at $\{111\}\langle 112\rangle$. The maximum intensities along the γ fiber are much lower than those along the α fiber. At 0 deg (*i.e.*, conventional rolling), the variation of intensity along the γ -fiber is not obvious (intensities are all around 3, indicating a continuous fiber texture),

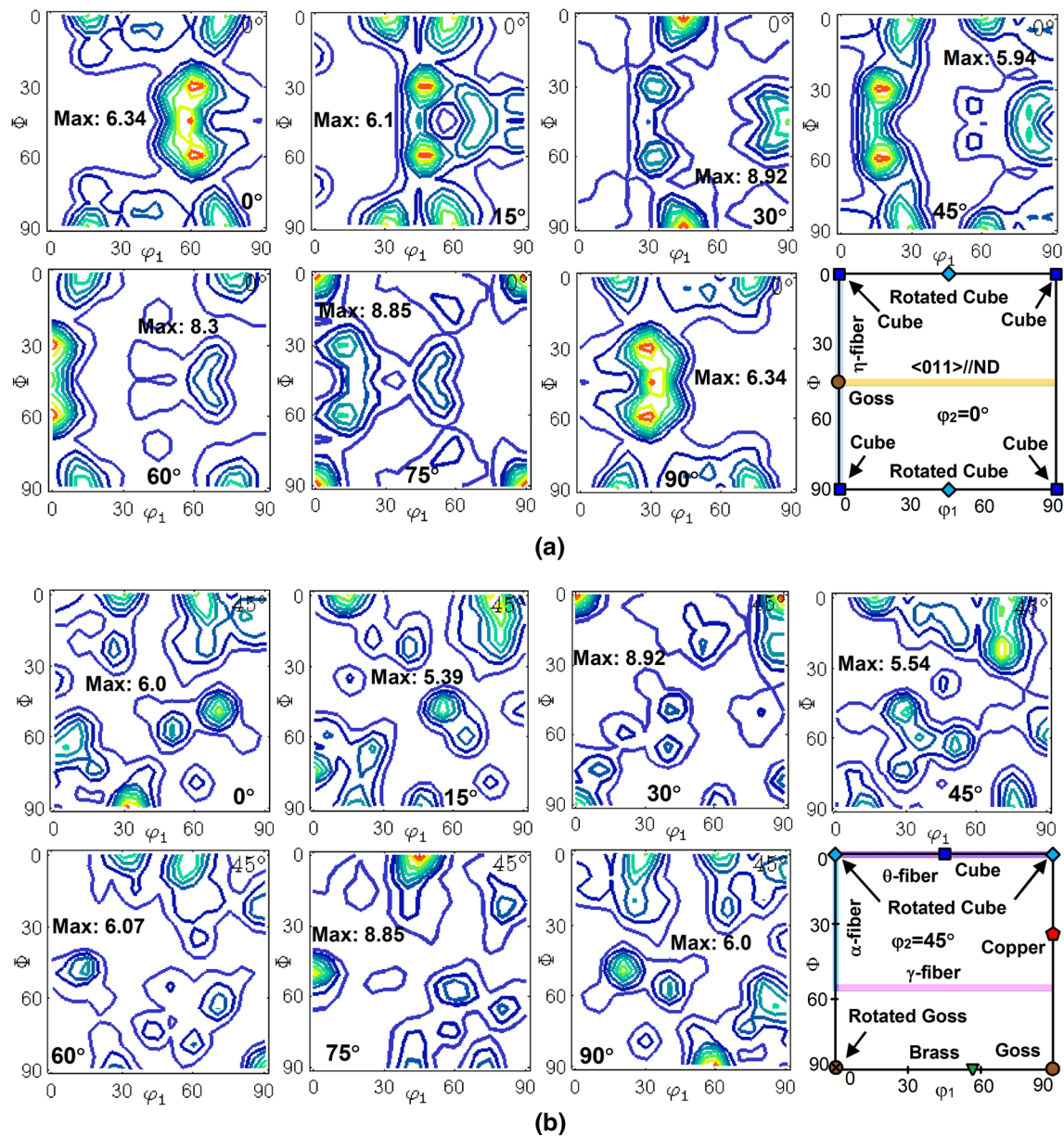


Fig. 6—Initial textures before cold rolling, obtained by rotations around the normal direction by 0 to 90 deg: (a) $\phi_2 = 0$ deg, and (b) $\phi_2 = 45$ deg sections of the ODF's (Bunge's notation).

while all the other angles show significant difference along this fiber. Thus, the inclination of CRD to HRD has a substantial effect on the γ -fiber, mainly by intensifying the $\{111\}\langle 110 \rangle$ orientations and weakening the $\{111\}\langle 112 \rangle$ components. Figure 8(c) shows the calculated volume fractions of the α and γ fibers at different inclination angles. While the volume fraction of the γ -fiber does not seem to be significantly affected by the inclination angle (all around 10 to 12 pct), the variation in α -fiber is remarkable. With the increase of the inclination angle, the α fiber volume fraction increases from about 30 pct to a maximum of ~ 40 pct at 75 deg and drops to about 30 pct again when the angle reaches 90 deg (cross rolling). The increase of the α -fiber volume fraction is mainly due to the increase of the rotated cube and the $\{112\}\langle 110 \rangle$ components.

C. Annealing Microstructure and Texture

Figure 9 shows the microstructures of the samples after final annealing at 1053 K (780 °C) for 2 hours. Like in the case of hot band annealing, there are large differences in grain size, *i.e.*, diameters from a few tens of micrometers to hundreds of micrometers in all the inclination angles. The average grain size varies from about 128 to 151 μm (~ 20 pct difference), and a rotation of 30 deg leads to the largest average grain size. At 45 and 75 deg inclination angles, the grain sizes are at minimum, which are close to the conventional rolling case (0 deg). The relatively small grain size in these two angles may be attributed to the relatively high density of dislocations (shear bands) accumulated during cold rolling (Figure 5). According to classic recrystallization

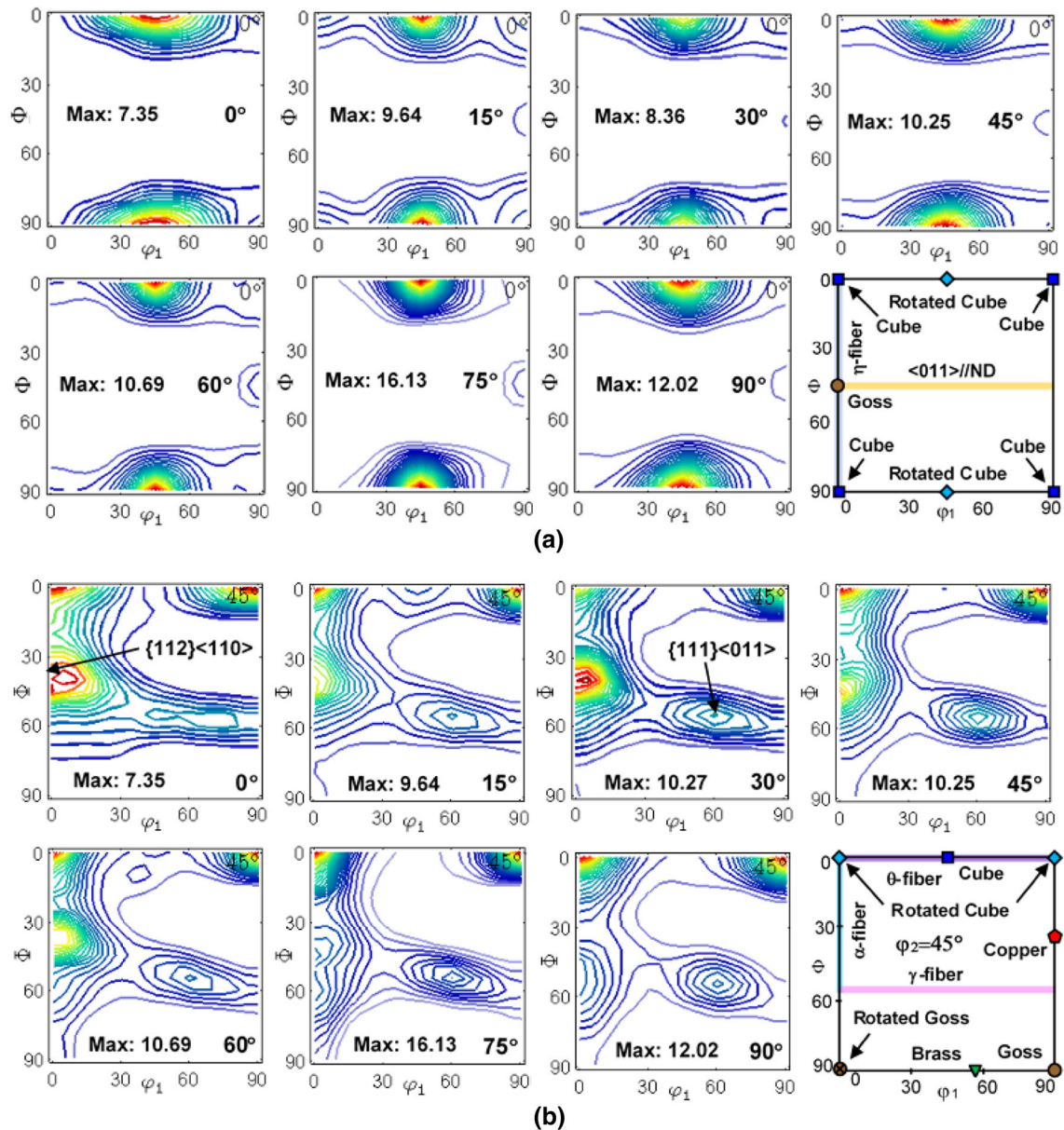


Fig. 7—Textures after cold rolling at various angles with respect to the hot rolling direction: (a) $\phi_2 = 0$ deg, and (b) $\phi_2 = 45$ deg sections of the ODF's (Bunge's notation).

theory,^[27] the nucleation rate and the number of nucleation sites are closely related to the density of dislocations (shear bands) and the deformation modes, which determine the heterogeneities and orientation gradients necessary to provide nucleation sites. A higher amount of shear bands (dislocations) leads to a larger number of nuclei and hence a smaller grain size.

Figure 10 shows the textures obtained after final annealing. Recrystallization considerably randomizes the textures, and the intensities are rather low compared to the cold-rolling textures. As seen from Figure 8, the inclination of the CRD to HRD (from 15 to 90 deg) produced much stronger cold-rolling textures than conventional rolling (0 deg), but these strengthened deformation textures do not produce a stronger recrystallization texture. Indeed, the recrystallization textures

at all the inclined angles are weaker than conventional rolling (0 deg) except at 60 deg, where a much stronger recrystallization texture is observed. This is contrary to the textures of low carbon steel processed by conventional rolling, where increasing the rolling strain usually leads to a stronger cold-rolling texture, which upon annealing gives rise to a stronger recrystallization texture.^[4] An outstanding feature of the annealing textures obtained using the current process is the formation of the θ -fiber ($\{001\} \perp \text{ND}$) and the disappearance or weakening of the α -fiber. This is significantly different from the recrystallization textures observed in most bcc metals (including electrical steels) processed using conventional rolling, where a decrease in the intensities of the $\{001\}$ orientations and an increase of the strength of the $\{110\}$ components along the α -fiber

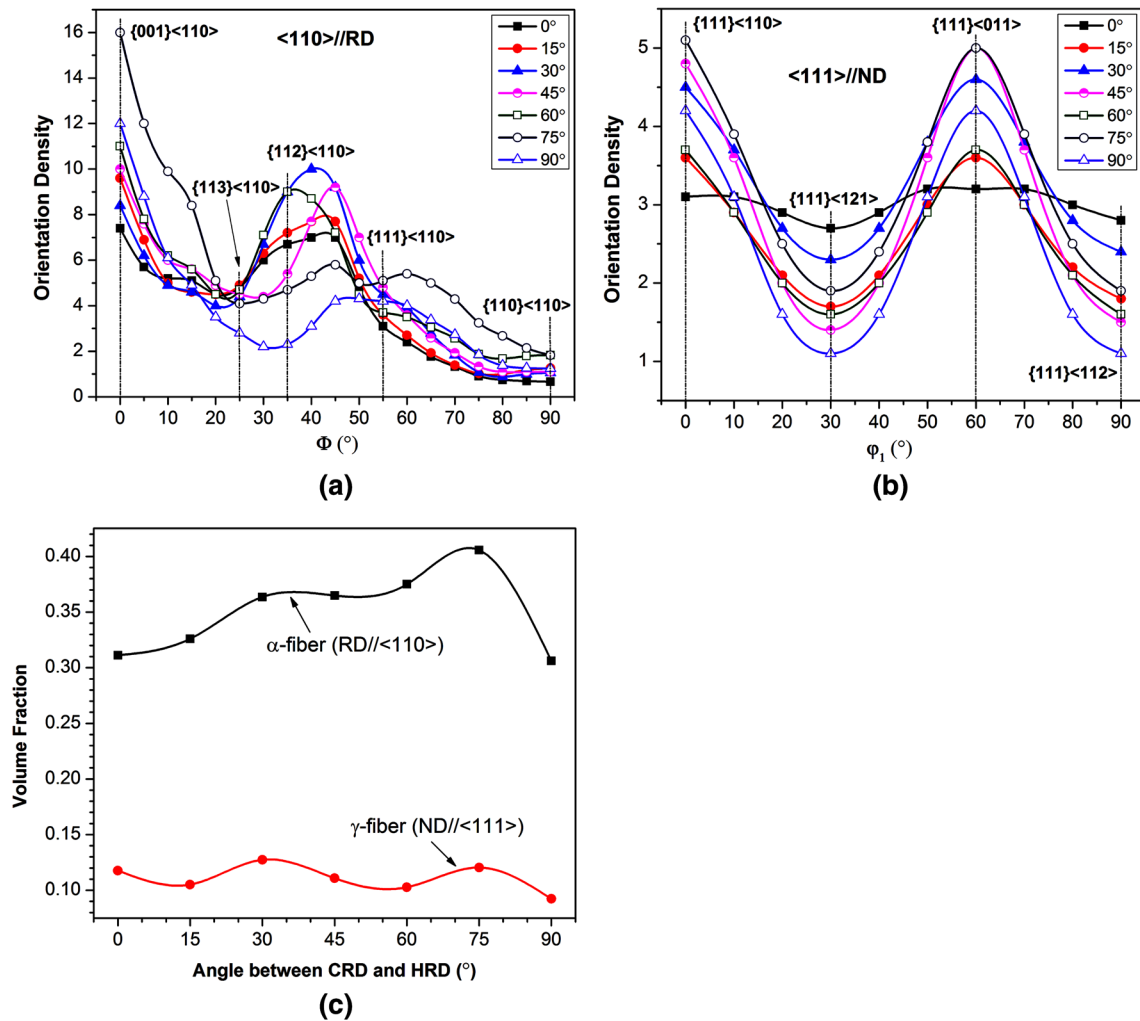


Fig. 8—Plot of the (a) α -fiber, (b) γ -fiber, and (c) volume fractions of the α - and γ -fibers with respect to the inclination angle between CRD and HRD after cold rolling.

were usually observed.^[27] It is noted that the γ -fiber is also significantly weakened, which either changes to a couple of discrete peaks close to $\{111\}\langle 112 \rangle$ and $\{554\}\langle 225 \rangle$ (15, 30, and 45 deg inclination angles) or essentially disappeared (75 and 90 deg).

In the current process, a θ -fiber also develops at 0 deg (conventional rolling), but the maximum intensity is at an orientation close to $\{110\}\langle 118 \rangle$, which is 10 deg away from the Goss orientation. No continuous γ -fiber is observed; instead, two minor peaks at $\{667\}\langle 6\ 13\ 6 \rangle$ and $\{554\}\langle 225 \rangle$ near the γ -fiber develop. Increasing the inclination angle to 15 deg weakens the overall texture, but the θ -fiber has been relatively intensified as the intensity is almost the same as the maximum intensity developed at the $\{110\}\langle 118 \rangle$ orientation. The $\{667\}\langle 6\ 13\ 6 \rangle$ and $\{554\}\langle 225 \rangle$ components near the γ -fiber are also weakened. Increasing the inclination angle to 30 deg further weakens the overall texture, but the peaks at $\{111\}\langle 112 \rangle$ are intensified and become the maxima. There is also another peak near $\{881\}\langle 3\ 5\ 16 \rangle$, an orientation about 20 deg away from the Goss component.

When the inclination angle increases to 45 deg, the θ -fiber essentially changes to a single-cube component

with some spread around it (maximum intensity is 3.35). The overall intensity is higher than 15 and 30 deg, and is close to conventional rolling (0 deg). A Goss texture clearly develops, which spreads from the exact Goss orientation to approximately the $\{110\}\langle 112 \rangle$ (brass) component. The γ -fiber is significantly weakened and almost diminishes. At an inclination angle of 60 deg, a remarkable intensity maximum (with a much higher intensity than all the other inclination angles) develops at the exact *cube* orientation, which was rarely achieved in electrical steels using conventional processing techniques. This maximum is surrounded by orientations along the θ -fiber up to $\{011\}\langle \frac{1}{2}\sqrt{3}\ 0 \rangle$, an orientation 15 deg away from the rotated cube. The γ -fiber degrades to two weak peaks (intensities of 1.6 and 1.4 only) close to the $\{111\}\langle 121 \rangle$ and $\{554\}\langle 225 \rangle$ orientations. A texture near $\{110\}\langle 2\ 2\ 11 \rangle$ also develops, which is located almost middle way between the brass and the Goss components in the $\langle 110 \rangle // ND$ fiber.

When the angle is increased to 75 deg, the texture intensity decreases again to 3.12, and the single strong cube maximum splits into two weaker peaks (the

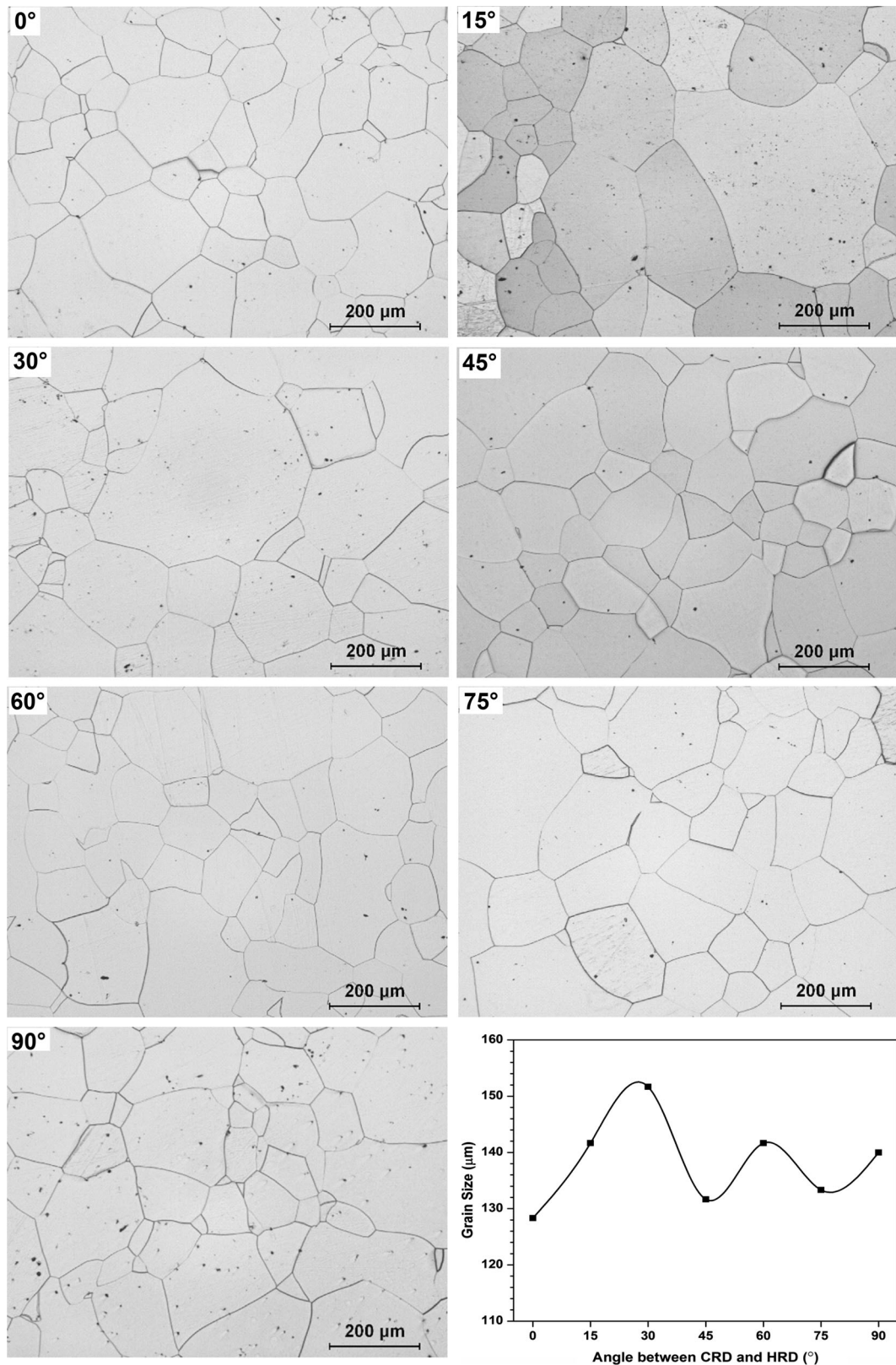


Fig. 9—Optical micrographs after final annealing at 1053 K (780 °C) for 2 h in Ar. Also shown is the average grain size (diameter) vs inclination angle between the CRD and HRD.

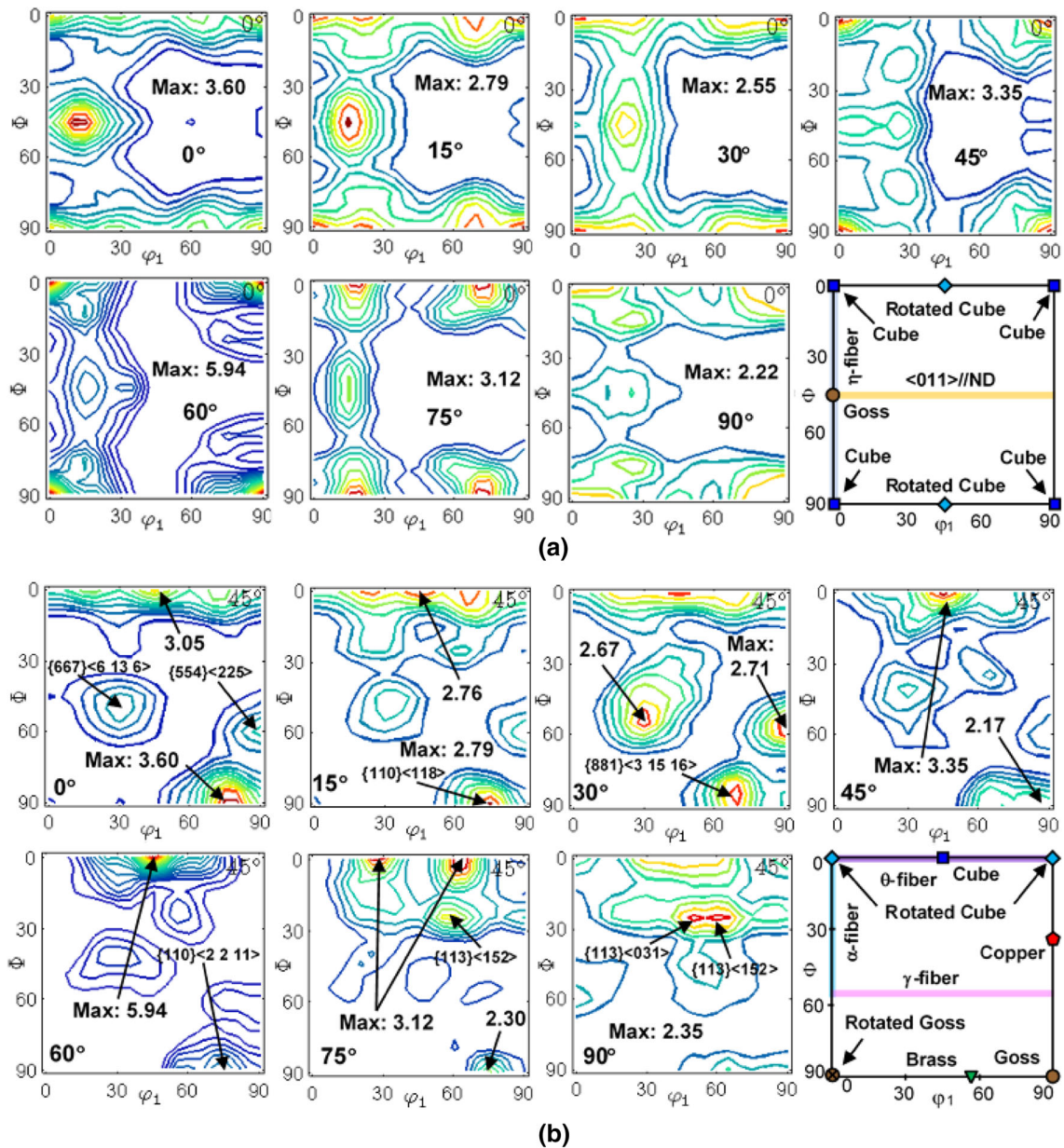


Fig. 10—Recrystallization textures after cold rolling at various angles with respect to the hot rolling direction: (a) $\varphi_2 = 0$ deg, and (b) $\varphi_2 = 45$ deg sections of the ODF's. Samples were annealed at 1053 K (780 °C) for 2 h after 2 pct skin pass rolling. Note a strong *cube* texture develops when the inclination angle is 60 deg.

$\{001\}\langle 130 \rangle$ orientations) about 20 deg away from the cube orientation along the θ -fiber. A texture near the $\{113\}\langle 152 \rangle$ orientation also develops, which is usually not observed in bcc metals after conventional rolling and recrystallization. The γ -fiber disappears, but the $\{110\}\langle 2\ 2\ 11 \rangle$ component remains. When the inclination angle reaches 90 deg (cross rolling), the intensity drops to the lowest value of 2.35, and a partial $\{113\}\perp$ ND fiber develops. The maxima are located at $\{113\}\langle 031 \rangle$ and $\{113\}\langle 152 \rangle$. A relatively strong texture (intensity 2.2) also develops around the exact cube orientation and spreads to the $\{001\}\langle 140 \rangle$ orientations (15 deg from the cube). The γ -fiber vanishes and the components between the brass and Goss orientations essentially disappears as well.

These features are seen more clearly in Figure 11, where the variations of intensity along the three most important fibers (θ , η , and γ) in the final annealed samples are plotted. It is emphasized that the 60 deg inclination angle significantly promotes the development of the cube component, while the 30 deg inclination angle enhances the γ fiber. Compared to conventional rolling (0 deg), a 45 deg inclination angle also produces relatively strong cube and Goss textures, and considerably reduces the γ -fiber intensities.

D. Texture Factor

To evaluate the effect of texture on magnetic properties of non-oriented electrical steels, the volume

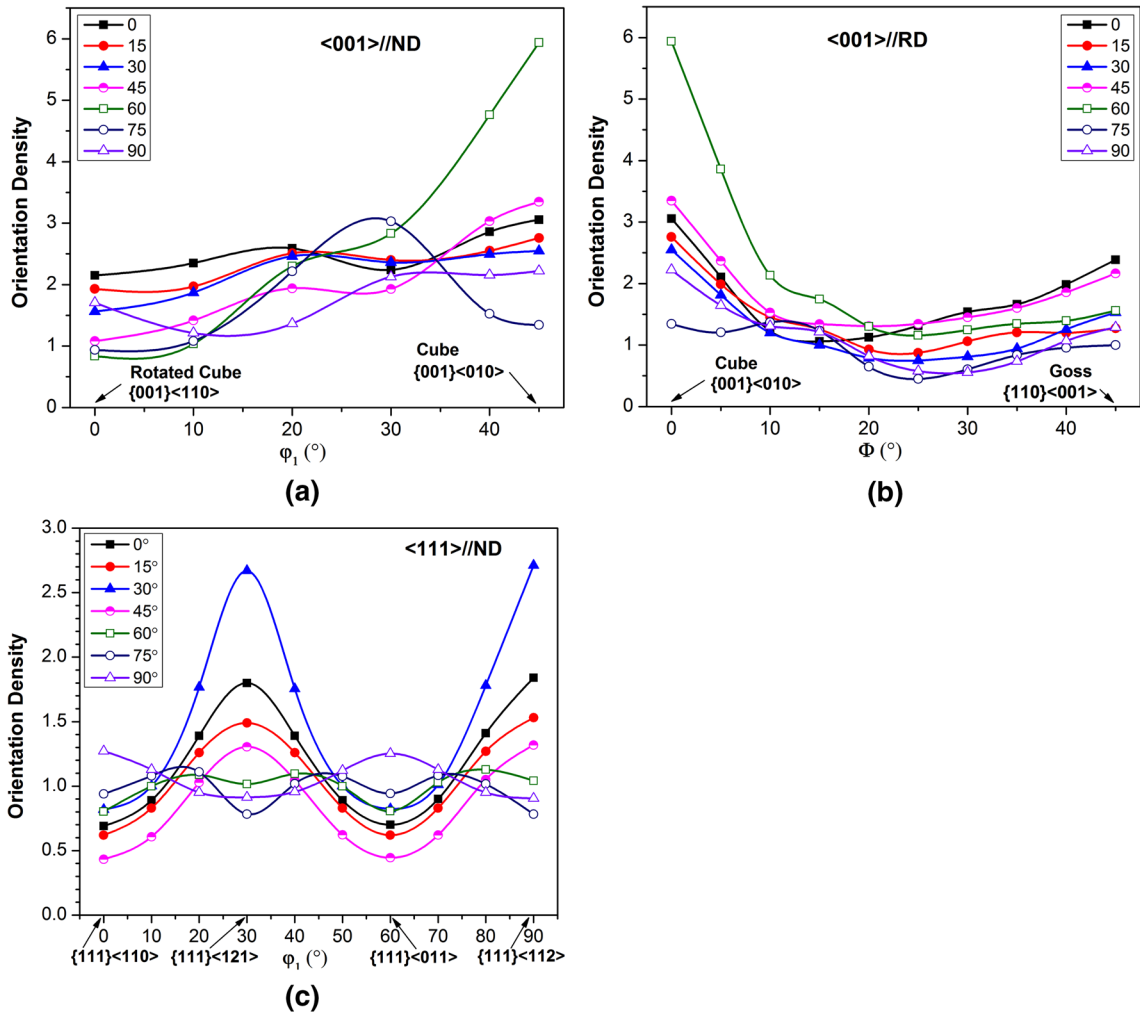


Fig. 11—Variation of intensity along (a) θ -fiber, (b) η -fiber, and (c) γ -fiber of the final annealed sheets cold rolled at various angles with respect to the hot rolling directions.

Table II. Volume Fractions (pct) of the Cube and Goss Texture Components and the γ Fiber

Inclination Angle	0 deg	15 deg	30 deg	45 deg	60 deg	75 deg	90 deg
Cube	3.3	3.3	3.0	3.9	4.4	3.4	3.5
Goss	4.3	2.7	2.8	3.3	2.8	2.4	2.3
γ fiber	12.8	10.9	14.6	12.1	11.2	10.1	11.6
(Cube + Goss)/ γ	0.60	0.55	0.40	0.59	0.65	0.57	0.50

fractions of specific texture components or fibers are usually calculated for quantitative comparison. Using a tolerance angle of 15 deg, the volume fractions of the cube, Goss and the γ -fiber are computed and listed in Table II. In conventional electrical steel processing, the volume fraction of the γ -fiber dominates the final texture, with volume fractions in the range of 40 to 50 pct,^[28] while in the current processing scheme, this only accounts for about 10 to 15 pct, *i.e.*, more than three times lower than conventional processing. The volume fractions of the cube component produced in this new processing scheme are close to those produced by conventional processing, *i.e.*, about 3.0 to 4.4 vs ~5.0

pct, but the Goss component has much higher volume fractions in the current process, *i.e.*, 2.3 to 4.3 vs 0.7 to 1.4 pct, an approximately three-time increase. It is thus clear that the processing technology proposed in this study can indeed significantly optimize the crystallographic textures of non-oriented electrical steel by significantly reducing the γ -fiber while increasing the Goss texture in the annealed sheets.

Figure 12 shows the variation of the texture factors, *i.e.*, the ratio of the favorable textures to unfavorable textures, with respect to the inclination angle. For non-oriented electrical steel, the cube texture is a favorable texture because it has two $\langle 001 \rangle$ directions

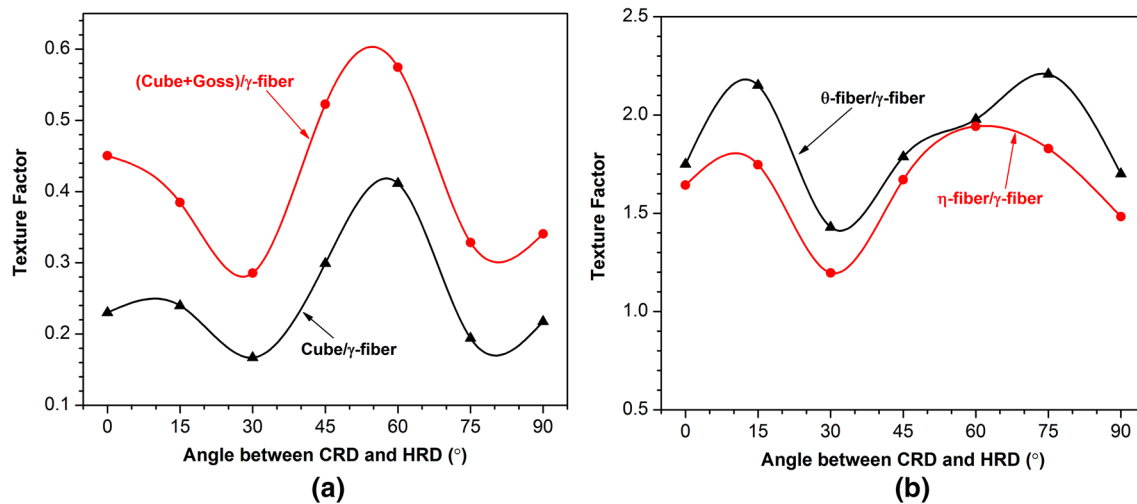


Fig. 12—Texture factors of the final annealed steel sheets vs the angle between CRD and HRD: (a) factors of specific components, and (b) factors of fibers.

on the sheet plane and will improve the magnetic properties in both the RD and TD directions. The Goss texture is also considered as a favorable texture as it has the $\langle 001 \rangle$ direction along the rolling direction, which will also improve the magnetic properties. The γ -fiber, which includes any orientations that have their $\{111\}$ planes parallel to the sheet, is detrimental to the magnetic properties and is unfavorable.

For conventional electrical steel processing, the texture factor, *i.e.*, typical ratio of cube to γ -fiber, was about 0.10 to 0.13,^[28] while in the current processing scheme, this factor is 0.2 to 0.4, and a maximum texture factor (0.4) is achieved when the inclination angle is 60 deg (Figure 12(a)). If both the cube and Goss textures are included in the texture factor, the ratios of cube plus Goss to γ -fiber will be much higher (3 to 4 \times) than conventional processing, *i.e.*, 0.4 to 0.65 vs 0.12 to 0.16. It is thus noted that the inclination angle has a remarkable effect on the texture factor. At an angle of 60 deg, both the cube/ γ -fiber and the (cube + Goss)/ γ -fiber ratios reach the maximum values, which are favorable for magnetic properties. At an angle of 30 deg, these factors have the minimum values, which will be detrimental to the magnetic properties.

Figure 12(b) shows the variation of the ratios of the η - and θ -fibers (the two magnetically favorable fibers) to the γ -fiber with respect to the inclination angle. Generally, at all the inclination angles, the θ -fiber/ γ -fiber ratio is higher than the η -fiber/ γ -fiber ratio. The 30 deg inclination angle gives rise to the lowest texture factors for both η -fiber/ γ -fiber and θ -fiber/ γ -fiber, and the 60 deg angle generates the maximum factor for the η -fiber/ γ -fiber factor. An inclination angle of 75 deg produces the highest θ -fiber/ γ -fiber factor.

IV. DISCUSSION

For grain-oriented electrical steels, a sharp $\{110\}\langle 001 \rangle$ texture (Goss)—a magnetically favorable orientation for

applications in transformers, had been produced through a complex thermomechanical process that involved conventional rolling, recrystallization, and a secondary recrystallization process (abnormal grain growth).^[29] In the case of non-oriented electrical steels for rotating machine applications, the ideal texture— $\{001\}\langle 100 \rangle$ (cube) has rarely been successfully produced through conventional rolling and recrystallization processes. A few special techniques such as cross-rolling,^[19,20] surface annealing,^[30] columnar-grain growth,^[3,31,32] phase transformation,^[33] *etc.* have been attempted, but these processes are very difficult to be applied in industrial production. Recent investigations using twin-roll casting plus high temperature annealing^[34] produced promising results on the formation of cube recrystallization texture in non-oriented electrical steels, but the texture shown in the research^[34] was not exactly the cube, but an orientation about 15 deg away from the $\{001\}\langle 100 \rangle$ along the θ -fiber.

Due to its technological and scientific importance, recrystallization texture has been the topic of extensive research for a few decades.^[27] It is known that the final recrystallization texture is highly dependent on the processing history of the material before annealing, as well as the annealing condition itself. Due to the metallurgical mechanisms that govern those processes, the textures obtained after conventional rolling and annealing processes do not promote the cube texture development.^[19] The final recrystallization texture was normally dominated by the unfavorable γ -fiber. In the present study, the effect of the initial texture on the cold rolling and final annealing textures was investigated by simply inclining the CRD to the HRD by an angle. This change of CRD with respect to HRD gives rise to a different starting texture that conventional hot rolling may not be able to produce, since after conventional hot rolling and annealing, the texture is normally dominated by the α - and γ -fibers.^[7] The technique used in this study provides a potential approach to control the cold rolling and recrystallization textures through the alteration of the starting texture.

As shown in Figure 6, the strongest texture (intensity 6.34) in the annealed hot band is $\left\{0\frac{1}{2}\frac{\sqrt{3}}{2}\right\}\left\langle\frac{1}{2}\frac{3}{4}\frac{\sqrt{3}}{4}\right\rangle$ (on the $\varphi_2 = 0$ deg section), in which the $\left\{0\frac{1}{2}\frac{\sqrt{3}}{2}\right\}$ plane is 15 deg from $\{011\}$ and 30 deg from $\{001\}$, while the $\left\langle\frac{1}{2}\frac{3}{4}\frac{\sqrt{3}}{4}\right\rangle$ direction is 60 deg from $\langle 100 \rangle$. Thus, when rotating the sample about the normal direction, the $\left\{0\frac{1}{2}\frac{\sqrt{3}}{2}\right\}$ plane is still parallel to the sheet plane, but the $\left\langle\frac{1}{2}\frac{3}{4}\frac{\sqrt{3}}{4}\right\rangle$ direction is gradually brought to the RD. Upon a 60 deg rotation, the $\left\{0\frac{1}{2}\frac{\sqrt{3}}{2}\right\}\left\langle\frac{1}{2}\frac{3}{4}\frac{\sqrt{3}}{4}\right\rangle$ orientation becomes $\left\{0\frac{1}{2}\frac{\sqrt{3}}{2}\right\}\langle 100 \rangle$, which is 15 deg away from the Goss component. The second strongest component (intensity 6.0) in the annealed hot band is $\{110\}\langle 665 \rangle$, which is located on the $\langle 110 \rangle$ //ND fiber. Its $\langle 665 \rangle$ direction is 30 deg from $\langle 110 \rangle$ and 60 deg from $\langle 100 \rangle$. A 30 deg rotation about the ND brings this to the rotated Goss orientation and a 60 deg rotation to the Goss orientation. The third strongest component in the original hot band is $\{001\}\langle 140 \rangle$ (intensity 4.5). Its $\langle 140 \rangle$ direction is ~30 deg from $\langle 110 \rangle$ and ~75 deg from $\langle 100 \rangle$. A 30 deg rotation transforms it to the rotated cube orientation and a 75 deg rotation to the cube orientation. These orientations contribute to the main textures after the rotations of the sample about the ND by 60, 30, and 75 deg.

It has been shown that, after a 30 deg rotation, the main feature of the starting texture was a strong $\{001\}\langle 110 \rangle$ (rotated Cube) component plus a relatively strong $\{110\}\langle 110 \rangle$ (rotated Goss) orientation. After cold rolling, the rotated cube intensity decreased slightly, while the orientation spread increased considerably. This is because the $\{001\}\langle 110 \rangle$ orientation is generally stable,^[35,36] but the rolling deformation of more than 70 pct reduction usually causes the decrease of its intensity as well as the spread of the orientation along the α -fiber.^[37] The strong cold rolling texture near $\{112\}\langle 110 \rangle$ can be attributed to the rotation of the $\{110\}\langle 110 \rangle$ orientation (rotated Goss) around the $\langle 110 \rangle$ axis in the rolling direction.^[37]

After a 75 deg rotation, the textures contained two strong components: $\{001\}\langle 100 \rangle$ (cube) and $\{667\}\langle 110 \rangle$, the latter being resulted from a 75 deg rotation of the $\{667\}\langle 3\ 11\ 12 \rangle$ orientation in the annealed hot band. After cold rolling, a very strong $\{001\}\langle 110 \rangle$ texture (intensity 16) was produced, which may be considered to be the result of a rotation of 45 deg of the cube orientation about the normal direction, as shown by Aspden.^[38] The $\{667\}\langle 110 \rangle$ orientation is ~4 deg away from $\{111\}\langle 110 \rangle$ and is on the α -fiber. Upon cold rolling, it rotates about the $\langle 110 \rangle$ axes lying in the rolling direction, and gives rise to the $\{111\}\langle 110 \rangle$ orientations as well as a spread along the $\varphi_1 = 0$ deg line ($\varphi_2 = 45$ deg section). The $\{111\}\langle 110 \rangle$ orientations are stable up to 85 pct reduction in thickness.^[37]

A 60 deg rotation gives rise to a maximum intensity at $\left\{0\frac{1}{2}\frac{\sqrt{3}}{2}\right\}\langle 100 \rangle$, an orientation located on the $\varphi_2 = 0$ deg section (not on the $\varphi_2 = 45$ deg section, as in the 30 and

75 deg cases). A second peak is found at the Goss orientation. Another component in the initial texture is $\{001\}\langle 140 \rangle$, which is a 15 deg rotation of the cube orientation around the $\langle 001 \rangle$ axes lying in the normal direction. The $\{001\}\langle 110 \rangle$ cold-rolling texture is resulted from the rotation of the near-cube orientations about the $\langle 110 \rangle$ axes in the normal direction. The Goss and near-Goss orientations change to $\{112\}\langle 110 \rangle$ and $\{111\}\langle 110 \rangle$ orientations through a rotation path that may consist of three stages of rotations: about the $\langle 110 \rangle$ axes in the transverse direction, about the $\langle 111 \rangle$ axes in the normal direction, and about the $\langle 110 \rangle$ axes in the rolling direction.^[37]

After rotations of 15, 45, and 90 deg around the normal direction, the textures are also altered, which resulted in the change of rotation paths of orientation flow during plastic deformation and thus different cold rolling textures. It should be noted that, although cross rolling (90 deg rotation) was included in this study, no significant enhancement of the cube texture (as has been shown in previous studies) in the final annealed sheet was observed. In fact, this inclination angle only produced a minor cube texture after annealing. This discrepancy was due to the fact that the cross rolling in this study was carried out using annealed hot bands, while the cross rolling in the previous investigation^[19] employed hot bands without annealing.

The recrystallization textures obtained in this study have a common feature that is different from many previous investigations: there is an apparent $\{001\}\perp$ ND texture in all the samples, some showing a continuous θ -fiber or discrete peaks, and others having a strong cube component. These recrystallization textures may be traced back to the initial textures before cold rolling, where after rotations about the plane normal, all the samples had some peaks along the θ -fiber. Although after cold rolling these became similar textures featured by a strong rotated cube orientation, they went back to the $\{001\}\perp$ ND orientations upon recrystallization (the intensity was considerably decreased though). The strongest cube texture obtained at a 60 deg inclination angle seemed to be related to the initial $\left\{0\frac{1}{2}\frac{\sqrt{3}}{2}\right\}\langle 100 \rangle$ orientation, as this was the strongest component in the initial texture and it did not exist in the initial textures of other inclination angles.

However, the strong rotated cube and cube textures obtained after 30 and 75 deg rotations, respectively, did not produce a strong final recrystallization texture; instead, some weak θ -fiber or $\{001\}\langle 130 \rangle$ textures were induced. Also, some minor components were found near the $\{111\}\langle 121 \rangle$ orientations, which were believed to recrystallize from the $\{112\}\langle 110 \rangle$ and $\{111\}\langle 110 \rangle$ orientations in the cold-rolling texture.^[13] It is noticed in this study that, a strong $\{112\}\langle 110 \rangle$ cold-rolling texture led to a strong $\{111\}\langle 121 \rangle$ texture after recrystallization, and if this orientation did not exist, as in the cases of 75 and 90 deg rotations, there was no $\{111\}\langle 121 \rangle$ component after recrystallization. Thus the $\{111\}\langle 121 \rangle$ recrystallization texture seemed to be originated from the $\{112\}\langle 110 \rangle$, not from $\{111\}\langle 110 \rangle$, since in the cases of 75 and 90 deg rotations, the $\{111\}\langle 110 \rangle$ still exists but there

is no $\{111\}\langle 121 \rangle$ after recrystallization. Although in the recrystallized samples the Goss texture is only found at inclination angles of 45 and 90 deg, there exists a near-Goss component (about 15 deg away from the exact Goss) in all the angles. This can be attributed to the formation of Goss or near-Goss nuclei in the shear bands within the deformed $\{112\}\langle 110 \rangle$ or $\{111\}\langle 110 \rangle$ grains,^[13] which exist in all the cold-rolled samples. Origins of the peaks at $\{113\}\langle 3\ 15\ 16 \rangle$ and $\{113\}\langle 031 \rangle$ as observed at the 75 and 90 deg rotations are not known.

It has been shown in this research that the cold rolling textures have essentially the same features no matter how much the starting textures differ. The difference is in the intensity of the overall texture and the relative intensities between the main texture components and fibers. The observed textures all resemble typical bcc rolling texture, which can be described by $\{001\}\langle 110 \rangle$, $\{112\}\langle 110 \rangle$, $\{111\}\langle 110 \rangle$ and $\{111\}\langle 112 \rangle$. Upon annealing, they all created some $\{001\}\perp\text{ND}$ components (the θ -fiber), and the only angle that produced a strong cube component (with an intensity approximately twice of the others) in the recrystallization texture was the 60 deg rotation. Although this has been attributed to the formation of the $\left\{0\frac{1}{2}\frac{\sqrt{3}}{2}\right\}\langle 100 \rangle$ initial texture by the 60 deg rotation of the annealed hot band, direct evidence has yet to be found to support this view.

The difference in the final annealing textures produced in this study may be attributed to the difference in the stored energy that has been introduced during the cold rolling of the initially same microstructure but different crystal orientations (and thus different orientation flow paths). The rotation of the samples not only gives rise to different macroscopic textures, but it also altered the orientations of the neighboring crystals of each grain, which imposed different grain boundary constraints during deformation. The result would be, at some angles (as in the 60 deg rotation case), the deformed neighboring grains may be beneficial to the nucleation and/or growth of the cube grains, which lead to the development of a strong cube texture in the final annealed sample. However, the exact mechanism that governs the formation of the cube texture at the 60 deg rotation has to be further investigated, e.g. by intensive EBSD analysis of the recrystallization process and by computer simulation of the texture evolution in the cold rolling process.

V. CONCLUSIONS

The CRD of a non-oriented electrical steel (0.88 wt pct Si) was intentionally inclined at various angles with respect to the HRD in order to alter the initial texture and orientation flow during cold deformation, and to affect the final annealing texture. Texture evolution after hot rolling, hot band annealing, cold rolling and final annealing was analyzed by EBSD and XRD, and it was found that the inclination of CRD to HRD has a significant effect on the final recrystallization texture. The findings can be summarized as:

After rotation of the hot band around the ND by an angle between 15 and 90 deg, not only the features of the

initial texture for cold rolling were altered, but the overall texture intensities were also changed (due to the pseudo-orthorhombic sample symmetry introduced during the calculations). At inclination angles of 30, 75, and 60 deg, the texture was considerably strengthened, while at angles of 15 and 45 deg, the intensity was slightly decreased.

Although with different starting textures, the resulted cold-rolling textures all had similar features, which resembled the typical cold-rolling texture of bcc metals produced by conventional rolling. The difference was the relative intensities between the main texture components and the α - and γ -fibers. A significant feature was the intensification of the rotated cube component and the weakening of the γ -fiber. At an inclination angle of 75 deg, a significantly strong-rotated cube texture was produced, which was more than double that produced by conventional cold rolling.

After final annealing, the recrystallization textures were all weakened, and the strongest cold-rolling texture (at 75 deg) did not produce the strongest annealing texture. A major character of the recrystallization texture produced using the proposed technique was the formation of the θ -fiber and the significant weakening of the γ -fiber. At an inclination angle of 60 deg, a very strong cube texture (intensity $\sim 2\times$ of conventional rolling) was produced in the final recrystallized sheet.

ACKNOWLEDGMENTS

Funding for this work was provided by Natural Resources Canada through the Program of Energy Research and Development (ecoEII ETRI011). United States Steel Corporation Research and Technology Center (Munhall, PA) is gratefully acknowledged for melting, hot rolling, and hot band annealing the steel plates. The authors are grateful to Michael Attard, Darren Bibby, Raul Santos, Renata Zavadil and Pei Liu for their contributions to this project. Peter Badgley from the United States Steel Corporation Canada (Hamilton, ON) is gratefully acknowledged for coordinating this research. Victoria Jarvis, McMaster Analytical X-ray Diffraction Facility, McMaster University, is thanked for the XRD texture measurements.

REFERENCES

1. F.J.G. Landgraf: *JOM*, 2012, vol. 64, pp. 764–71.
2. M. Getzlaff: *Fundamentals of Magnetism*, Springer, Berlin, 2008.
3. T. Tomida, S. Uenoya, and N. Sano: *Mater. Trans.*, 2003, vol. 44, pp. 1106–15.
4. L. Kestens and J.J. Jonas: *ASM Handbook, Part 1*, ASM International, Materials Park, 2005, vol. 14, pp. 685–700.
5. W.C. Jeong: *Mater. Lett.*, 2008, vol. 62, pp. 91–94.
6. B. Hutchinson, L. Ryde, and K. Tagashira: *Mater. Sci. Eng., A*, 1998, vol. A257, pp. 9–17.
7. J.J. Sidor, K. Verbeken, E. Gomes, J. Schneider, P.R. Calvillo, and L.A.I. Kestens: *Mater. Charact.*, 2012, vol. 71, pp. 49–57.
8. H. Yashiki and T. Kaneko: *J. Magn. Magn. Mater.*, 1992, vol. 112, pp. 200–202.
9. O. Fischer and J. Schneider: *J. Magn. Magn. Mater.*, 2003, vols. 254–255, pp. 302–306.

10. S. Akta, G.J. Richardson, and C.M. Sellars: *ISIJ Int.*, 2005, vol. 45, pp. 1666–75.
11. M. Takashima, M. Komatsubara, and N. Morito: *ISIJ Int.*, 1997, vol. 37, pp. 1263–68.
12. E.J. Gutierrez-Castaneda and A. Salinas-Rodriguez: *J. Magn. Magn. Mater.*, 2011, vol. 323, pp. 2524–30.
13. J. Park, J.A. Szpunar, and S.Y. Cha: *ISIJ Int.*, 2003, vol. 43, pp. 1611–14.
14. Y. Sidor, F. Kovac, and T. Kvackaj: *Acta Mater.*, 2007, vol. 55, pp. 1711–22.
15. T. Tomida and T. Tanaka: *ISIJ Int.*, 1995, vol. 35, pp. 548–56.
16. T. Nakayama, N. Honjou, T. Minaga, and H. Yashiki: *J. Magn. Magn. Mater.*, 2001, vol. 234, pp. 55–61.
17. M. de Campos, F.J.G. Landgraf, I.G.S. Falleiros, and G.C. Fronzaglia: *ISIJ Int.*, 2004, vol. 44, pp. 1733–37.
18. M.A. da Cunha and S.C. Paolinelli: *Mater. Res.*, 2002, vol. 5, pp. 373–78.
19. L. Kestens and S. Jacobs: *Texture Stress Microstruct.*, 2008, vol. 173083, pp. 1–9.
20. Y. Hayakawa and M. Kurosawa: *Acta Mater.*, 2002, vol. 50, pp. 4527–34.
21. G.F. Vander Voort: *Metallography Principles and Practice*, ASM International, Materials Park, 1999, pp. 447–53.
22. R. Hielscher and H. Schaeben: *J. Appl. Crystallogr.*, 2008, vol. 41, pp. 1024–37.
23. J. Hunady, M. Cernik, E.J. Hilinski, M. Predmersky, and A. Magurova: *J. Magn. Magn. Mater.*, 2006, vol. 304, pp. e620–23.
24. A.D. Rollett and S.I. Wright: *Typical Textures in Metals*, Cambridge University Press, Cambridge, 1998, pp. 179–237.
25. E. Aernoudt, P. Van Houtte, and T. Leffers: *Deformation and Textures of Metals at Large Strain*, John Wiley & Sons Canada Ltd., Toronto, 1992, pp. 89–136.
26. L.S. Toth, J.J. Jonas, D. Daniel, and R.K. Ray: *Metall. Trans. A*, 1990, vol. 21A, pp. 2985–3000.
27. F.J. Humphreys and M. Hatherly: *Recrystallization and Related Annealing Phenomena*, 2nd ed., Elsevier Ltd, Oxford., 2004.
28. S.K. Chang and W.Y. Huang: *ISIJ Int.*, 2005, vol. 45, pp. 918–22.
29. I.L. Dillamore and W.T. Roberts: *Metall. Rev.*, 1965, vol. 10, pp. 271–380.
30. C.G. Dunn and J.L. Walter: *Trans. Metall. Soc. AIME*, 1962, vol. 224, pp. 518–33.
31. N. Zhang, P. Yang, and W.M. Mao: *Mater. Lett.*, 2013, vol. 93, pp. 363–65.
32. F. Kovac, M. Dzubinsky, and Y. Sidor: *J. Magn. Magn. Mater.*, 2004, vol. 269, pp. 333–40.
33. T. Tomida: *J. Appl. Phys.*, 1996, vol. 79, pp. 5443–45.
34. Y.H. Sha, C. Sun, F. Zhang, D. Patel, X. Chen, S.R. Kalidindi, and L. Zuo: *Acta Mater.*, 2014, vol. 76, pp. 106–17.
35. P.K. Koh and G.C. Dunn: *Trans. Met. Soc. AIME*, 1955, vol. 203, pp. 401–405.
36. T. Taoka, E. Furubayashi, and S. Takeuchi: *Trans. Iron Steel Inst. Jpn.*, 1966, vol. 6, pp. 201–32.
37. H. Inagaki and T. Suda: *Texture*, 1972, vol. 1, pp. 129–40.
38. R.G. Aspden: *Trans. Met. Soc. AIME*, 1959, vol. 215, pp. 986–91.